Hydrogen Release and Microstructure of MgH$_2$ Based Composite Powders Containing a Relevant Amount of LaNi$_5$

N. Abazović[a,b,*], A. Aurora[a], V. Contini[a], M.R. Mancini[a], A. Montone[a]

and M. Vittori Antisari[a]

[a]ENEA FIM Department, C.R. Casaccia, Via Anguillarese 301, 00123 Rome, Italy

[b]Permanent address: Laboratory for Radiation Chemistry and Physics, Vinča Institute of Nuclear Sciences,

P.O. Box 522, 11001 Belgrade, Serbia

Micro-composite materials based on MgH$_2$ with the addition of a relevant amount of LaNi$_5$ have been synthesized by reactive ball milling. The powder microstructure has been studied by a combination of X-ray diffraction and scanning electron microscopy, while the decomposition behaviour and the hydrogen release properties have been obtained by differential thermal analysis and thermo-gravimetric measurements. Both temperature scans and constant temperature isotherms have been used to this purpose. Experimental results allow identifying optimum processing condition for synthesis of material that shows the onset of hydrogen release at temperatures as low as 450 K. The decomposition kinetics has been studied by isothermal measurements which show that the whole process cannot be described by just one mechanism limiting the reaction velocity. In fact in the first decomposition step the reaction is kinetically limited by the second phase nucleation, while, for partially decomposed samples the bulk diffusion appears to limit the process. On the basis of the experimental results we propose a mechanism of phase transformation where a percolating network of the two phases is formed.

PACS numbers: 61.05.cp, 61.82.Bg, 65.40.−b, 68.37.Hk

1. Introduction

MgH$_2$ shows several barriers for practical use in the hydrogen storage, mainly because it is characterized by high thermodynamic stability and slow decomposition kinetics [1–6]. The combination of these factors originates decomposition temperatures too high for most technological application so that the purpose of several research efforts is to find the way of facilitating the decomposition route of this compound.

In general, the formation/decomposition of a metal hydride consists of several basic steps: (1) dissociation/recombination of hydrogen molecule at the metal surface; (2) sub-surface penetration of H atoms; (3) hydrogen diffusion in the bulk of the material; (4) nucleation and growth of metal hydride/metal phase. The slowest step determinates the overall kinetic of the sorption/desorption process, which than can be often easily described by simple rate expressions [7, 8].

By adding metallic particles (Fe, Co, Ni, V) [7, 9–12], which are known to catalytically assist the H$_2$ molecule dissociation, hydrogen diffusion can be accelerated and the kinetic behaviour becomes limited by the nucleation

and growth of the new phase described by the Johnson–Mehl–Avrami model [7].

Improvements in (de)hydrogenation kinetics of MgH$_2$ were also obtained in systems where the oxides of some 3d transition elements (TiO$_2$, V$_2$O$_5$, Fe$_3$O$_4$, Mn$_2$O$_3$), were used as additives [13]. The mechanisms at the basis of the kinetics enhancements are not completely understood.

However the role of a second phase can be more complex, besides the simple catalyzing action, as recently have been shown by Barkhordarian et al. in their study of hydrogenation/dehydrogenation behaviour MgH$_2$–Nb$_2$O$_5$ composites [14]. In described case, the additive has a dual role: in fact, particles of Nb$_2$O$_5$ act as nucleation sites for new phase, assisting the first step of phase transformation to metallic magnesium and their presence at the MgH$_2$ surface improves the velocity of recombination of H atoms. As a consequence, very fast decomposition kinetics has been obtained, with a rate--limiting step represented by a velocity of the inter-phase surface which is well described by the contracting volume kinetic model.

Starting from similar considerations, in the present work we have investigated the behaviour of MgH$_2$–LaNi$_5$ composite materials. The experimental work is based on hypothesis that this intermetallic compound, once intermixed with MgH$_2$ can play at least two roles. From one

───────

* corresponding author; e-mail: `kiki@vinca.rs`

side it can protrude through the oxide/hydroxide surface layer, and owing to good hydrogen transport properties and acceptable atmosphere compatibility can give rise to an easy escape way for hydrogen gas. On the other hand, well distributed particles of $LaNi_5$ can behave as nucleation sites for metallic Mg during dehydrogenation process. This two functions require that the second phase particles are either relatively large, in order to protrude from surface crust, and well distributed in the MgH_2 bulk in order to provide a high density of nucleation sites. Consequently, a relatively large amount of this second phase has been added to MgH_2 making so necessary to find a compromise between the kinetic performances of the composite and the corresponding absolute hydrogen storage capacity.

Composite material has been synthesized by high energy ball milling, technique that, as it is very well known, can provide atomic level intimate contact between phases [15, 16]. In particular we have performed ball milling under hydrogen atmosphere, since, among other factors, it appears to promote a better distribution of the additive particles in the MgH_2 matrix.

In fact, the particle size distribution of the synthesized powder represents an important issue affecting the kinetic aspects and a reduction of the powder size can facilitate the hydride dissociation owing to the shorter diffusion distances involved in the phase transformation process and the larger specific surface. This aspect has been clearly elucidated by Aguey–Zinsou et al. [17] who showed that finely pulverized MgH_2 shows fast decomposition kinetics.

We report on the performances of MgH_2 composites containing a relatively large amount of $LaNi_5$ and showing significant improvement in dehydrogenation kinetics even after exposure to the atmosphere. The material has been carefully characterized from both the functional and the microstructural aspects with a particular attention to the determination of the reaction kinetics.

2. Experimental procedures

Magnesium hydride (MgH_2, 60 μm particle size, with 5% of Mg as impurity from Th. Goldschmidt) and $LaNi_5$ (50 μm particle size, from SAES GETTERS, 99%) powders were ball milled in a Spex Mixer/Mill 8000, under 8 bar H_2 atmosphere using specially designed hardened steel vials equipped with a needle valve (Cantil Srl), allowing evacuation and gas filling. Ball to powder ratio (BPR) has been set to 10:1. Mixtures MgH_2 — x wt.% $LaNi_5$ ($x = 10, 30$) were processed for different times (1, 3, 5, 10, 20 h). After milling, sample handling was done in glove box under Ar atmosphere. However, all the post-milling characterization analyses, including the thermal desorption tests, were performed after atmosphere exposure.

XRD patterns were obtained using Cu Kα radiation in a Bragg–Brentano powder diffractometer equipped with a graphite monochromator positioned in the diffracted beam.

Morphological and micro-analytical characterization was carried out by Scanning Electron Microscopy (SEM) with a Cambridge 250MKIII equipped with EDS microanalysis and backscattered electron detector. Cross-sectional samples, able to reveal the internal powder microstructure, were prepared by embedding powders in epoxy resin followed by polishing according to usual metallographic procedure. A thin carbon layer was vacuum deposited before SEM observations in order to prevent surface charging under electron beam irradiation.

MgH_2 thermal decomposition reaction and hydrogen desorption was investigated by thermo-gravimetric analysis and differential thermal analysis (TGA-DTA) simultaneously performed on Netzsch STA 409 under 99.9995% pure Ar flow by constant rate heating runs, performed at fixed heating rate of 10 °C/min. Detailed analysis of the reaction kinetics, with the aim of deriving information on the operating rate limiting step and on the corresponding activation energy, has been performed by isothermal experiments carried out at different temperatures.

3. Results and discussion

3.1. Structural and morphological analyses

X-ray diffraction analysis have shown that in the adopted conditions and for times here considered, the main effect of ball milling processing is, besides the usually reduction of particle size, formation of an amorphous phase. This is shown in Fig. 1 where an X-ray diffractogram relative to the sample $MgH_2 + 30$ wt.% $LaNi_5$ milled for 5 h is reported. The diffractogram evidences four main features: (a) a partial modification of MgH_2 from a tetragonal to an orthorhombic phase; (b) a small shift to low angle of the peaks belonging to the $LaNi_5$ phase which can suggest the formation of a $LaNi_{5-x}H_{0.15}$ phase [18]; (c) the presence of a broad peak characteristic of an amorphous phase; (d) peaks characteristic of fcc Ni.

The absence of further peaks indicates that no other new crystal phases deriving from the intermixing of $LaNi_5$ and Mg have been synthesized. The partial amorphization of $LaNi_5$ is not unexpected in the light of the observations of Fujii et al. [18] who were able to induce glass transformation of this phase by ball milling. According to their findings, ball milled $LaNi_5$ begins to lose the crystal order immediately, so that the amorphous fraction is notable even after 1 h of processing. In our case, this phase transformation appears to proceed more slowly, probably owing to the less energetic conditions of our milling procedure. We agree with the suggestions of Fujii et al. that the amorphous phase can incorporate some hydrogen and be deficient in Ni having so a general formula $LaNi_yH_x$ (with $y < 5$) considering the high affinity of La for hydrogen, constituting the ball milling atmosphere, and the presence of crystalline Ni reflections in the X-ray diffractograms. Besides, increasing the milling time, the X-ray diffractograms (not reported) never have shown presence of new crystalline phases containing La.
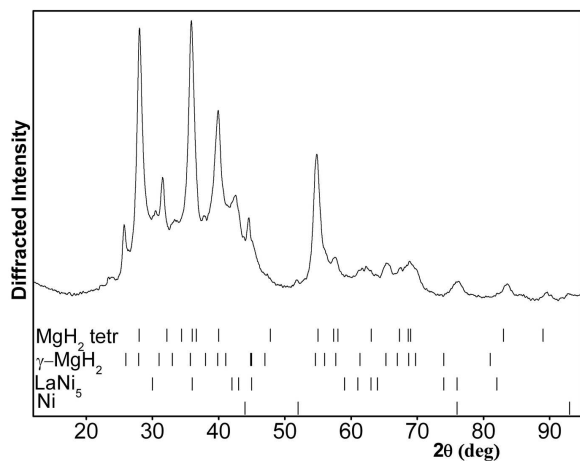
Fig. 1. X-ray diffraction pattern of the sample containing 30 wt.% LaNi$_5$ and milled for 5 h (tetr. stays for tetragonal).

Structural modifications and decomposition under the action of the milling process of the LaNi$_5$ phase are the main reason for setting an upper limit to the processing time. In fact, in this peculiar case, the milling time should be set on the basis of a compromise between structural refinement, in terms of particle pulverization and dispersion of the second phase in the MgH$_2$ matrix, and phase destabilization. As it will be discussed later, this feature is reflected also in the decomposition temperatures of the composite, which, after a strong decrease for short term milling, begins to increase again after 10–20 h of processing. Our study was so limited at 20 h of ball milling.
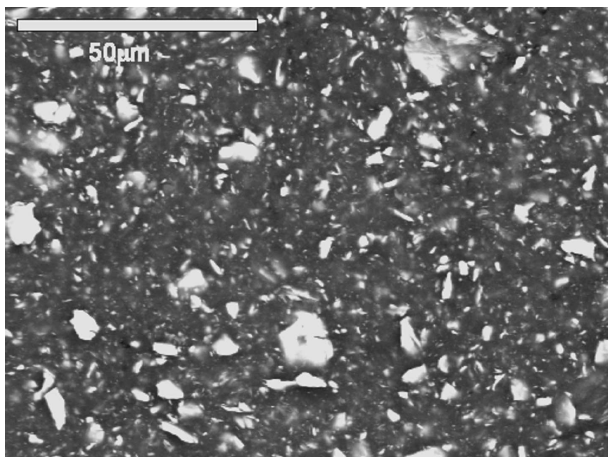

Fig. 2. SEM backscattered electron image of the cross section of the sample containing 30 wt.% LaNi$_5$ and milled for 5 h.

An example of the powder particle microstructure is shown in Fig. 2, where back-scattered electron images of polished cross sections of powder specimen containing 30% LaNi$_5$ milled for 5 h is reported. The sample is constituted by a micro-composite where the LaNi$_5$ particles, having a brighter contrast, are homogeneously distributed into the MgH$_2$ phase matrix.
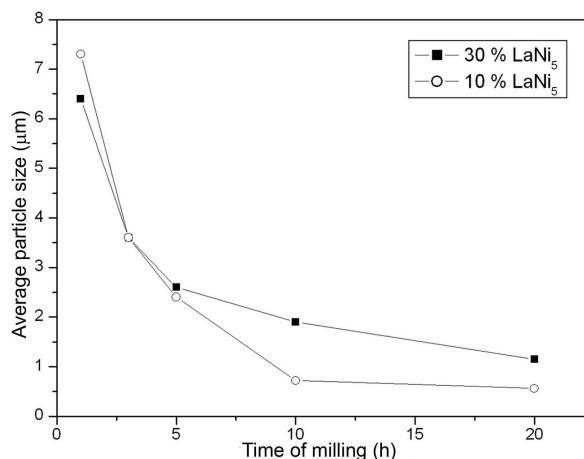

Fig. 3. LaNi$_5$ average particle size versus the milling time for the two analyzed compositions.

The repeated ball impacts induce a noticeable size refinement of the LaNi$_5$ particles, whose evolution with the milling time is reported in Fig. 3. It is possible to notice that the pulverization effect appears to be stronger when a smaller amount of LaNi$_5$ additive is present.

Summarizing the results of the microstructural characterization, it is possible to report that up to 5 h of processing time the sample microstructure can be schematized, at a first approximation, as a homogeneous dispersion in the MgH$_2$ matrix, of partially amorphous LaNi$_y$H$_x$ particles having a size decreasing with the milling time. No new crystalline phases can be detected, even if it is not possible to exclude the partial incorporation of Mg in LaNi$_5$ based amorphous phase.

3.2. Thermal decomposition

Figure 4 shows differential thermogravimetry (DTG) desorption curves, obtained by heating at the constant rate of 10 K/min, relative to the set of samples constituted by MgH$_2$ doped with 10 wt.% of LaNi$_5$. In the figure are also reported, for comparison purposes, the DTG curves relative to pure MgH$_2$ both as received and ball milled for 10 h. For all the reported curves, the differential thermal analysis (DTA) data, obtained simultaneously, confirm the DTG results. Both kind of analyses evidence a strong reduction of desorption temperature and point out a complex dehydrogenation behaviour which generally comprises more than one event dominating the process at different temperatures.

With an additive concentration of 10%, after 1 h of milling the thermal decomposition of MgH$_2$ onsets at about 490 K and exhibits more than one broad peak. The presence of more than one component appears to be a common feature of several experimental situations. By increasing the milling time to 3 h and 5 h the kinetics
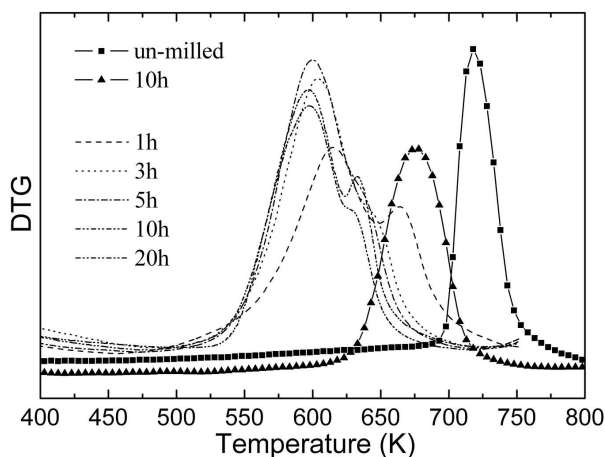
Fig. 4. DTG curves for $MgH_2 + 10\%$ $LaNi_5$ (line) in comparison to pure MgH_2 (line + symbol) at different time milled under Argon atmosphere at heating rate of 10 K/min.

of desorption process is fastened and we observe a reduction of desorption temperatures. A further increase in the milling time to 10 h and 20 h does not improve the desorption kinetics and the hydrogen amount in the highest temperature peak appears reduced.
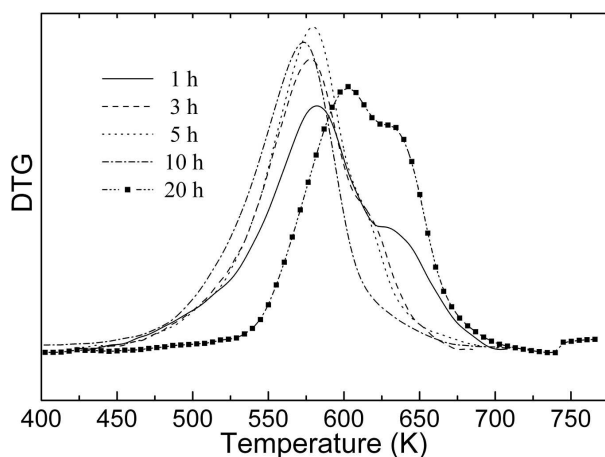

Fig. 5. DTG curves for $MgH_2 + 30\%$ $LaNi_5$ at different time milled under Argon atmosphere at heating rate of 10 °C/min.

This behaviour is confirmed by the results, reported in Fig. 5, relative to the sample doped with 30 wt.% of $LaNi_5$. In fact, the main features are not qualitatively different from what just described, since the samples show a fast dehydrogenation process after short term milling and performance deterioration for milling times larger than 10 h. Also in this case the observed desorption curves appear to be constituted by the convolution of more than one elementary phenomenon. However, it is possible to observe a marked improvement of the de-

hydrogenation kinetics with respect to samples with a smaller amount of additive. In fact, even after a very short term milling of 1 h, the thermal decomposition begins at about 450 K and to increase the milling time up the 10 h does not appear to affect appreciably the low temperature part of the desorption curve. A further increase in the milling time up to 20 h induces, also in this case, marked kinetics degradation. Actually, the whole desorption curve is shifted at higher temperature indicating a loss of the efficiency of the second phase contribution.

In order to provide a more quantitative description of the experimental results, the elementary curves constituting the DTG experimental data have been separated, by considering simple Gaussian components in a deconvolution process, an example of which is reported in Fig. 6. The results of the analysis, in terms of temperature and amplitude of the single components are reported in Table I.
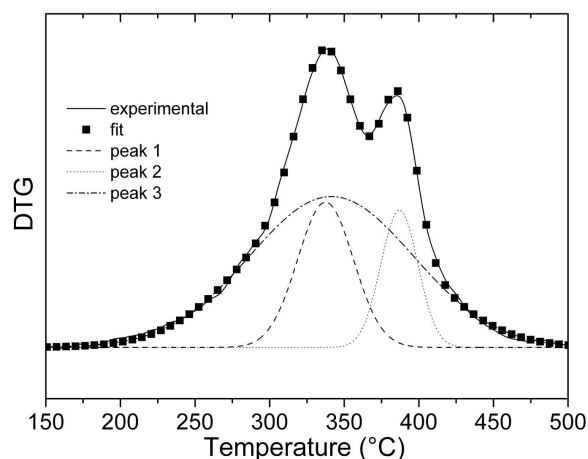

Fig. 6. DTG plot for $MgH_2 + 10\%$ $LaNi_5$ milled for 1 h with deconvolution of curve into single peaks.

From the whole set of data and from the comparison between samples with different amounts of additive we can conclude that the addition of $LaNi_5$ to MgH_2 improves the kinetics of thermal decomposition which occurs so at lower temperatures.

The experimental results seem to evidence the presence of two effects with opposite influence on the desorption kinetics. In fact, the milling process induces a fast dehydrogenation in first steps of the process, while prolonged milling induces marked performance deterioration. An interpretation of this behaviour can be attempted on the basis of the microstructural characterization, and we can make the hypothesis that the first effect, improving the desorption properties is related to the fragmentation and to homogeneous dispersion of the additive in the MgH_2 matrix, while the second effect can be related to the structural modification of $LaNi_5$ phase evidenced by X-ray diffraction, or to an excessive fragmentation of these catalyzing particles. Since

both phenomena, microstructural refinement and LaNi$_5$ amorphization, proceed with ball milling we can explain the presence of a time window where the material shows optimum performances. However, really optimum performances are obtained only when a sufficient amount of

additive is present, besides adopting the proper processing time. In fact, only for the samples constituted by MgH$_2$ + 30 wt.% of LaNi$_5$ processed for a time between 3 h and 5 h optimum kinetic performances are obtained.

TABLE I

TG\DTG data at different time milled of MgH$_2$ + 10% LaNi$_5$ and MgH$_2$ + 30% LaNi$_5$.

	90:10				70:30			
	$T_{\text{onset}}(k)$	$T_p(k)$	$T_p^*(k)$	wt.%	$T_{\text{onset}}(K)$	$T_p(K)$	$T_p^*(K)$	wt.%
1 h	493	610.2	614.3	65.2	450.9	583.6	571.1	56.9
		657.4	610.4	21.4		639	582.1	30.1
			659.9	13.4			640.5	13
3 h	506.5	603.8	595.1	48.1	450.8	577	557.1	59
		644.4	600.7	40.4		615.8	579	35
			641.6	11.5			620.9	6
5 h	493	597.5	590.5	38.3	465.1	579.5	569.8	60
		633	594	34.2		616.8	578.5	37
			621.3	27.4			618.4	2
10 h	500.6	592.6	591.8	73	471.9	574.8	551.6	57.6
		622.1	593.7	23			574.8	38.4
			628.1	4			639.5	4.0
20 h	503	592.8	593.3	83.3	528.3	600.9	602.2	79.4
		625.4	597.2	2.9		635.3	641.8	12.1
			631.1	7.9			664.1	6.7
			666.2	5.9			506.6	1.8

Tonset and T_{P}: data obtained from TG curve T^*p and wt.%: Temperature peak and percent of hydrogen desorption obtained from the deconvoluted DTG curve.

The comparison between samples with different amount of additive and processed for the same time allows us to make further considerations on the features of the additive particles which can be useful in assisting the dehydrogenation process. Let us consider the situation after 5 h of ball milling. The average particle size, as reported in Fig. 3, is roughly the same for both additive contents. This means that for 10% of additive, the density of catalyzing particles is about $1/3$ than in samples having 30% of additive. The comparison of the corresponding decomposition kinetics evidences that a smaller density of additive particles is less efficient in inducing fast decomposition kinetics. We can so infer that the interparticle average distance plays an important role, mainly in decreasing temperature of the decomposition process. This point will be discussed later together with the results of the kinetics measurements.

3.3. Kinetic measurements

The kinetics of decomposition reaction during isothermal treatment was measured with the aim of determin-

ing the rate limiting step of the decomposition process. This set of measurement concerns the samples showing optimum performances constituted by MgH$_2$ containing 30 wt.% of LaNi$_5$ and ball milled for 3 h and 5 h.

In a generic phase transformation, the reaction rate can be expressed as:

$$\frac{d\alpha}{dt} = k(T)f(\alpha). \tag{1}$$

For isothermal reactions $k(T)$ becomes a constant and the equation (1) can be easily integrated leading to:

$$g(\alpha) = \int_0^\alpha \frac{d\alpha}{f(\alpha)} = kt, \tag{2}$$

where α is the reacted fraction at time t, k is the rate constant, which temperature dependence can be generally described by the Arrhenius law $k = A\exp(-E/RT)$ with A is a frequency factor, E the activation energy, R is the gas constant and T the absolute temperature; $f(\alpha)$ and $g(\alpha)$ are the functions depending on the reaction mechanism.

TABLE II

Solid-state reaction mechanisms.

Mechanism	Function $g(\alpha)$
F1 — Random nucleation with one nucleus/particle	$-\ln(1-\alpha)$
F2 — Random nucleation with two nuclei/particle	$1/(1-\alpha)$
A2 — Nucleation and growth (Avrami equation 1)	$-\ln(1-\alpha)^{-1/2}$
A3 — Nucleation and growth (Avrami equation 2)	$-\ln(1-\alpha)^{-1/3}$
A3 — Nucleation and growth (Avrami equation 3)	$-\ln(1-\alpha)^{-1/4}$
D1 — One-dimensional diffusion	α^2
D2 — Two-dimensional diffusion	$(1-\alpha)\ln(1-\alpha)$
D3 — Three-dimensional diffusion (Jander)	$(1-(1-\alpha)^{-1/3})^2$
D4 — Three-dimensional diffusion (Ginstling-Brounshtein)	$1-(2/3)-(1-\alpha)^{-2/3}$
R2 — Phase boundary reaction (contracting area)	$1-(1-\alpha)^{1/2}$
R3 — Phase boundary reaction (contracting volume)	$1-(1-\alpha)^{1/3}$

Figure 7 shows $\alpha - t$ isothermal plots obtained during decompositions at 453 K and 573 K. The function describing the decomposition kinetics has been determined at both temperatures, by fitting the experimental data concerning $\alpha - t$ to the set of functions reported in Table II. The function fitting in the best way the data, determined by the last square method, has been considered indicative of the process step limiting the decomposition kinetics.

This kind of analysis shows that not all the desorption curves can be fitted by considering only one mechanism; in particular the desorption experiments carried out at temperatures lower than 500 K evidence the presence of at least two mechanisms, limiting the process in different stages of the reaction. This finding is more evident in the lower temperature curves where the sequence of desorption steps can be more easily separated. In this temperature range, in a first time, when the material is mainly constituted by MgH$_2$ the reaction rate can be well fitted by a function

$$g(\alpha) = -\ln(1-\alpha)$$

indicating that instant random nucleation of metallic Mg in the bulk of MgH$_2$ phase represents the rate limiting step of the reaction. Later on, when the fraction of metallic Mg is sufficiently high, a diffusion process controls the reaction kinetics.

The MgH$_2$/Mg ratio at which we observe the change in the mechanism limiting the decomposition reaction, depends on the milling time. In fact, considering the test temperature of 453 K, in the sample milled for 3 h, the diffusion process becomes dominant when 56% of the whole hydrogen content is desorbed, while for 5 h of milling the turnover point appears to be set at 82% of MgH$_2$ decomposition. Of course, turning point depends also on the temperature, probably owing to the different activation energies of the two mechanisms, even if
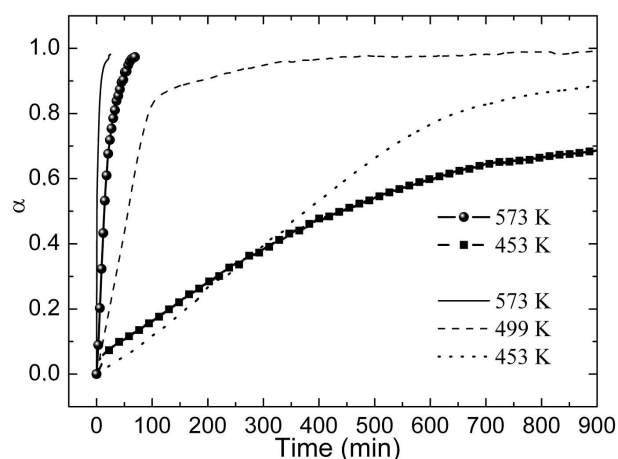

Fig. 7. $\alpha(t)$ curves for MgH$_2$+30% LaNi$_5$ milled for 3 h (line + symbol) and 5 h (line) respectively at different temperatures.

the general trend on the basis of which specimens milled for a longer time change later the desorption mechanism is confirmed. We have to notice that for temperatures higher than 500 K the first mechanism appears to controls the reaction for whichever composition of the sample indicating that probably in this case the temperature is high enough to impart fast transport properties to whichever microstructure generated during the decomposition process.

A possible explanation of low temperature behaviour can be based on the consideration that the hydrogen diffusion through the structure becomes more sluggish by increasing the fraction of metallic Mg, so that it begins to control the reaction kinetics when the diffusion length in this last phase reaches a critical value. This critical value depends, besides the temperature, on the characteristics

of the ball milling processing. In fact, a longer process inducing a finer dispersion of the additive and a more refined microstructure, helps in imparting fast transport properties also when a larger fraction of the sample is constituted by metallic Mg.

In the first part of the decomposition process, when the nucleation is the slowest process step, the hydrogen can easily diffuse to the powder particle surface indicating that the refined MgH$_2$ microstructure easily assists the hydrogen mass transport. We can make hypothesis that a nucleation process distributed through the structure can give rise to a strongly interconnected microstructure with the different phases constituting percolating networks with a large area of inter-phase boundary as already proposed in the interpretation of similar results [8]. In fact this consideration is supported also by the fact that a shorter inter-particle distance related to a larger amount of additive imparts better properties to the microstructure. Combining the information on the rate limiting step with the better properties of the material having a larger particle density we can infer that the nucleation of the Mg phase occurs at the additive particles. It appears so that a strongly interconnected microstructure can impart fast hydrogen transport properties to the material necessary for the diffusion of hydrogen at the powder particle surface. We can infer that fast transport can occur at the boundary between the hydrated and the metallic phase where a hydrogen deficient hydride can be present. Such phase has been experimentally observed during MgH$_2$ decomposition and it appears quite natural to expect a location at the Mg–MgH$_2$ boundary. The fast transport properties could be related to the presence of hydrogen vacancies in the structure able to support the jump of hydrogen atoms, which can so occur with a larger frequency.

Summarizing this aspect, we can make the hypothesis that a distributed nucleation in the structure, supported by the additive particles, induces a percolating microstructure with a high inter-phase specific area where fast diffusion paths can be located. This can explain the fastening of the transport step in the first part of the MgH$_2$ decomposition. This interpretation provides also a simple explanation to the change in the rate limiting step for partially de-hydrogenated samples. In fact, when the metallic Mg constitutes the most of the sample microstructure, the inter-phase area is forced to decrease and the diffusion process is forced to occur through the metallic Mg. This change difference can explain why hydrogen diffusion becomes the rate limiting step for heavily de-hydrogenated samples.

It is interesting to notice that the absolute desorption rate does not depend on the particular sample during the first part of the curve, when nucleation is controlling the kinetics, indicating that probably the underlying physico-chemical mechanism is not depending on the details of the microstructure.

In order to better characterize the first part of the process, we have estimated the activation energy from the
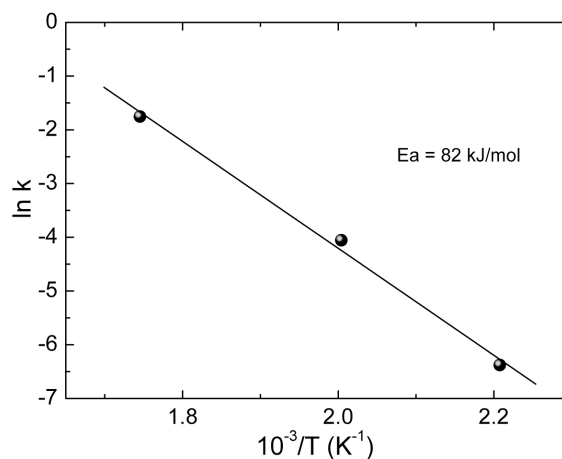

Fig. 8. Arrhenius plot of the constant reaction rates of MgH$_2$ + 30% LaNi$_5$ milled for 5 h.

Arrhenius plot reported in Fig. 8. Computed value of the apparent activation energy is 80 kJ/mol, which is considerably lower when compared with 156 kJ/mol, representative of MgH$_2$ non-activated by ball milling and also when compared with 120 kJ/mol often observed by pure ball milled MgH$_2$ [19–21]. This result appears to indicate that the LaNi$_5$ particles play an important role in defining the reaction rate limiting step and its activation energy.

4. Conclusions

The addition of LaNi$_5$ to MgH$_2$ and the processing by ball milling in hydrogen atmosphere give rise to composite powder particles able to release hydrogen with fast kinetics at relatively low temperatures. In fact, decomposition reaction, for the optimum additive content and for the proper processing conditions, onsets at about 450 K and it is fast enough to release most of the hydrogen content in about 60 s at 573 K.

The main effect of the milling process is, beside the usually observed structural refinement and additive dispersion in fine particles, the partial amorphization of the LaNi$_5$ phase. However optimum performances are obtained for short term milling when this phenomenon is just at the beginning in our experimental conditions, so that the reflections belonging to the LaNi$_5$ crystal phase are still dominating in the X-ray diffraction pattern.

Optimum desorption conditions, are obtained only when 30 wt.% of LaNi$_5$ is added to MgH$_2$, indicating that both, density and the average size of the additive particle, are playing a role in determining the kinetics of the MgH$_2$ decomposition reaction.

Kinetic analysis of isothermal decomposition runs indicates a complex behaviour with a rate limiting step constituted by the nucleation in the first stages of the reaction and a kinetic limitation due to the hydrogen diffusion process when the samples are heavily de-hydrogenated.

The concentration at which the second mechanism becomes dominant is depending on the microstructure, and longer ball milling with a more refined microstructure allow keeping the surface recombination limitation for a more de-hydrogenated sample. The recombination of hydrogen atoms into the bi-atomic molecule appears to occur at the surface of the $LaNi_5$ phase owing to activation energy sensibly smaller than the one observed on MgH_2.

The structural refinement allows proposing an interpretation of the fast diffusion of hydrogen in the structure based on the presence of a hydrogen deficient phase at the inter-phase boundary in a percolating structure already considered in similar systems.

In conclusion, the addition of $LaNi_5$ appears so to facilitate hydrogen release by assisting several steps of the thermal decomposition reaction of MgH_2.

References

[1] L. Schlapbach, A. Züttel, *Nature* **414**, 353 (2001).

[2] M. Fichter, *Advanced Engineering Materials* **7**, 443 (2005).

[3] A. Zaluska, L. Zaluski, J.O. Ström-Olsen, *Appl. Phys. A* **72**, 157 (2001).

[4] F.C. Gennari, F.J. Castro, G. Urretavizcaya, *J. Alloys Comp.* **321**, 46 (2001).

[5] D. Fátay, Á. Révész, T. Spassov, *J. Alloys Comp.* **399**, 237 (2005).

[6] S.R. Johnson, P.A. Anderson, P.P. Edwards, I. Gameson, J.W. Prendergast, M. Al-Mamouri, D. Book, I. Rex, J.D. Harris, A. Speight, Walton, *Chem. Commun.* **22**, 2823 (2005).

[7] G. Liang, J. Huot, S. Boily, R. Schulz, *J. Alloys Compd.* **305**, 239 (2000).

[8] N. Bazzanella, R. Checchetto, A. Miotello, *App. Phys. Lett.* **85**, 5212 (2004).

[9] A. Bassetti, E. Bonetti, L. Pasquini, A. Montone, J. Grbovic, M. Vittori, Antisari, *Eur. Phys. J.B* **43**, 19 (2005).

[10] A. Montone, J. Grbovic, Lj. Stamenkovic, A.L. Fiorini, L. Pasquini, E. Bonetti, M. Vittori, Antisari, *Mater. Sci. Forum* **518**, 79 (2006).

[11] A. Zaluska, L. Zaluski, J.O. Ström-Olsen, *J. Alloys Comp.* **289**, 197 (1999).

[12] A. Glage, R. Ceccato, I. Lonardelli, F. Girardi, F. Agresti, G. Principi, A. Molinari, S. Gialanella, *J. Alloys Comp.* **478**, 273 (2009).

[13] G. Barkhordarian, T. Klassen, R. Bormann, *Scr. Mater.* **49**, 213 (2003).

[14] G. Barkhordarian, T. Klassen, R. Bormann, *J. Alloys Comp.* **407**, 249 (2006).

[15] J. Hout, G. Liang, R. Schulz, *App. Phys. A* **72**, 187 (2001).

[16] A. Ye. Yermakov, N.V. Mushnikov, M.A. Uimin, V.S. Gaviko, A.P. Tankeev, A.V. Skripov, A.V. Soloninin, A.L. Buzlukov, *J. Alloys Comp.* **425**, 367 (2006).

[17] K.-F. Aguey-Zinsou, J.R. Ares, T. Fernandez, R. Klassen, Bormann, *Materials Research Bulletin* **41**, 1118 (2006).

[18] H. Fujii, S. Munehiro, K. Fujii, S. Orimo, *J. Alloys Comp.* **330-332**, 747 (2002).

[19] N. Hanada, T. Ichikawa, J. Fujii, *J. Phys. Chem. B* **109**, 7188 (2005).

[20] T.R. Jensen, A. Andreasen, T. Vegge. J.W. Andreasen, K. Ståhl, A.S. Pedersen, M.M. Nielsen, A.M. Molenbroek, F. Besenbacher, *Int. J. Hydrogen Energy* **31**, 2052 (2006).

[21] J. Huot, G. Liang, S. Boily, A. Van, R. Neste, Schulz, *J. Alloys Comp.* **293-295**, 495 (1999).